Magnesium Clusters: Structural and Electronic Properties and the Size-Induced Nonmetal-to-Metal Transition†

Julius Jellinek* and Paulo H. Acioli‡

Chemistry Division, Argonne National Laboratory, Argonne, Illinois 60439

Received: April 3, 2002; In Final Form: July 24, 2002

Structural and electronic properties of neutral and anionic magnesium clusters with 2 to 22 atoms are studied using gradient-corrected density functional theory. A new scheme for the conversion of the Kohn−Sham eigenenergies into electron binding energies is utilized to compute the difference in the binding energies of the two most external electrons in the anionic clusters. The results are in very good agreement with the data obtained in recent electron photodetachment experiments. The other electronic properties studied include (a) the binding energy, the second difference of the total energies, the HOMO−LUMO gap, and the vertical ionization potential of the neutral clusters; (b) the vertical electron detachment energy of the anionic clusters; and (c) the character of bonding in both the neutral and the anionic clusters. The analysis focuses on the finite-size analogue of the insulator-to-metal transition. The role and manifestation of the finite-size effects are discussed, and some important implications regarding the interpretation of the experimental data are pointed out.

1. Introduction

Metal clusters, or more precisely, atomic clusters of elements that are metals in bulk quantities, form an area of special interest.[1] Apart from the direct relevance to many technologies, they exhibit a host of novel features and phenomena not found in clusters of other elements. One of these is the change in the nature of bonding as a function of the cluster size. In fact, small atomic clusters of metallic elements may altogether lack characteristics usually associated with the metallic state. These characteristics then grow in as the clusters grow in size.[2] Is the transition to metallicity monotonic or not? What is the typical size or size-range at which it takes place? The answers to these questions are sketchy at best. The phenomenon is complex and multifaceted because different properties evolve differently with size. Therefore, the apparent onset and manifestations of the transition may depend on the property studied. The task is to identify and understand those size-induced changes in the different properties that can be viewed as the finite-size analogue of the bulk insulator-to-metal transition.

Magnesium, similarly to beryllium and mercury, is especially appropriate for the investigation of the size-induced transition to metallicity. Whereas the diatomic molecule of magnesium is a weakly bonded van der Waals system, magnesium clusters of larger sizes exhibit strong bonding. The structural and electronic properties of magnesium clusters have been investigated theoretically utilizing different quantum chemical and density functional theory (DFT) approaches.[3−13] The quantities used to interrogate the transition to the metallic state include the gap between the highest occupied molecular orbital (HOMO) and the lowest unoccupied molecular orbital (LUMO), the degree of *p*-character of the valence electronic charge,[5,8,13] the distribution of the electron charge density, the changes in the nearest-neighbor bond lengths,[5,8] the similarity with the jellium model picture,[6] the electronic density of states,[8] and the excitation energies.[12] The changes in these quantities with the cluster size were interpreted as consistent with the emergence of metallic attributes. However, because of the lack of appropriate experimental data, the results of the computations remained unverified. Even more importantly, the general subject of the finite-size specificity of the transition and of the ways it exhibits itself remained largely unexplored.

The goal of this study is to reexamine the structural and electronic properties of small magnesium clusters with the above-mentioned issues in mind. An added impetus for such a reexamination is furnished by two recent experimental explorations. In the first,[14] mass-spectra of Mg_n^+, $n \leq 80$, have been measured and used to analyze the corresponding neutral clusters in the context of the jellium model. Invoking compatibility with the jellium picture as a signature of metallic behavior, the authors concluded that the smallest magnesium cluster that exhibits such behavior is Mg_{20}. In the second exploration,[15] photoelectron spectroscopy (PES) measurements on Mg_n^-, $n = 3-35$, clusters were used to evaluate the difference between the binding energies of the two most external electrons. This difference was viewed as the HOMO−LUMO gap in the corresponding neutral clusters, and the reduction and eventual closure of this gap was invoked as the criterion of the transition to metallicity. The measurements showed that the difference in the binding energies of the two most external electrons indeed decreases with the size of the Mg_n^- clusters and becomes zero at or around $n = 18$.[15] The decrease, however, is not monotonic, and nonzero values of the difference reemerge at some larger anion-cluster sizes.

We utilize a gradient-corrected version of the DFT. In the next section, we present the results of the tests used to select the exchange and correlation functionals and the pseudopotential/basis set. In section 3, we recap our recently formulated scheme[16] for converting the Kohn−Sham (KS) eigenenergies into electron binding energies. Results on the structural and

† Part of the special issue "R. Stephen Berry Festschrift".

* To whom correspondence should be addressed. Tel: (630) 252-3463. Fax: (630) 252-4954. E-mail: jellinek@anl.gov.

‡ Permanent address: Instituto de Física, Universidade de Brasília, Brasília, DF, 70919-970, Brazil.

10.1021/jp020887g CCC: $22.00
Published on Web 10/11/2002

TABLE 1: Comparison of the Present All-Electron DFT Results (BP'86, BPW91, and B3LYP) with Those of Earlier ab Initio (CCSD(T) and MP2−R12) and Experimental (exp) Studies[a]

system	property	BP86	BPW91	B3LYP	CCSD(T)	MP2−R12	exp
Mg	IP (eV)	7.731	7.529	7.751			7.646[e]
	EA (eV)	< 0	< 0	< 0			unstable
Mg_2	r_e (Å)	3.562	3.527	3.919		3.891[d]	3.891[f]
	D_e (eV)	0.091	0.099	0.016		0.057[d]	0.049[f]
Mg_3	r_e (Å)	3.295	3.275	3.480	3.387[b]	3.387[d]	
(D_{3h})	D_e (eV)	0.41	0.46	0.13	0.25[b]	0.33[d]	
Mg_4	r_e (Å)	3.103	3.094	3.180	3.110[b]	3.110[d]	
(T_d)					3.103[c]		
	D_e (eV)	1.21	1.33	0.55	1.04[b]	1.37[d]	
					1.14[c]		

[a] The DFT computations are performed with the 6-31G* basis Set. The MPW1PW91 functional yields results similar to those of BPW91. IP is the ionization potential, EA is the electron affinity, r_e is the equilibrium interatomic distance, and D_e is the dissociation energy. [b] Ref 3a. [c] Ref 3b. [d] Ref 3c. [e] Ref 21. [f] Ref 22.

TABLE 2: Comparison of the BP'86 DFT Results Obtained within Two Pseudopotential and an All-Electron Treatments[a]

		pseudopotential		
system	property	WH[b]	Stuttgart[c]	all-electron
Mg	IP (eV)	7.803	7.812	7.731
	EA (eV)	< 0	< 0	< 0
Mg_2	r_e (Å)	3.560	3.633	3.562
	D_e (eV)	0.091	0.073	0.091
Mg_3	r_e (Å)	3.282	3.361	3.295
(D_{3h})	D_e (eV)	0.47	0.34	0.41
Mg_4	r_e (Å)	3.082	3.155	3.103
(T_d)	D_e (eV)	1.25	1.02	1.21
Mg_5	r_e (Å)	3.005[d]	3.072	3.018
(D_{3h})		3.333	3.407	3.330
	D_e (eV)	1.52	1.25	1.53

[a] The notations are the same as in Table 1. [b] Ref 19. [c] Ref 23. [d] The first number is the bond length between two "waist" atoms and the second between a waist atom and an apex atom of the trigonal bipyramid (cf. Figure. 3).

energy characteristics of the anionic and neutral Mg_n, $n = 2-22$, clusters are presented in section 4. Their electronic features, as obtained in the computations, are given and discussed in section 5. The discussion includes comparisons with the experimental PES data and an analysis of the interpretation of these data regarding the finite-size analogue of the insulator-to-metal transition. Some general remarks on the specificity of this transition in the finite-size regime are summarized in section 6.

2. Computational Details

The computations are performed within the DFT with the Becke exchange[17] and Perdew correlation[18] functionals (BP'86), and using unrestricted, for open-shell cases, and restricted, for closed-shell cases, wave functions. The valence electrons (two per each Mg atom) are described by a (21|21) basis set. The remaining ionic cores are represented by the Wadt−Hay pseudopotential.[19] The BP'86 exchange-correlation functional emerged as the optimal in test studies on Mg_n, $n = 1-4$, performed using all-electron computations with the 6-31G* basis set.[20] The other functionals considered include BPW91, B3LYP, and MPW1PW91, as implemented in the Gaussian98 program. The performance of the functionals was evaluated against the available quantum chemical and experimental data (cf. Table 1). Two pseudopotential/basis set choices, that of Wadt and Hay[19] and of Fuentealba et al.[23] (the "Stuttgart pseudopotential"), were tested within the BP'86 approach. The results of the BP'86 all-electron treatment were used as a basis for judgment. As indicated by the data in Table 2, the two choices yield overall comparable results, with the Wadt−Hay pseudopotential performing somewhat better.

The search for the stable structural forms was performed for both the neutral and the anionic clusters. Gradient-based techniques were used, and a variety of initial guess configurations, including asymmetric ones, was considered for each cluster size. The energy minimization included all degrees of freedom. Normal-mode analysis was applied to filter out those stationary structures that correspond to saddle points, rather than minima, of the corresponding potential energy surfaces.

The optimization of the structures also provides the structure-specific electronic features. Among these are the ones that correspond to the native configurations of the clusters (the term "native" denotes here the most stable configuration of a cluster of a fixed size in a chosen charge state). Additional complete DFT computations were performed for each cluster size to obtain its electronic characteristics in the anionic, neutral, and cationic charge states, all considered in the native configurations of both the neutral and the anionic clusters. The discussion below (see section 5) clarifies the role of these additional computations in elucidating the meaning and implications of the measured PES data[15] in the context of the size-induced transition to metallicity, and in shedding light on the finite-size-specific aspects of the phenomenon. On the technical side, these additional computations are needed for conversion of the DFT KS eigenenergies into electron binding energies as described in the next section.

3. Conversion of Kohn−Sham Eigenenergies into Electron Binding Energies

One of the central goals of this study, prompted by the recent PES experiments[15] (cf. section 1), is to compute the binding energies of the two most external electrons in anionic magnesium clusters. To accomplish this within a DFT treatment one has to correct the (negative of the) KS eigenenergies because they correspond to auxiliary particles rather than to electrons. A number of correction procedures have been suggested in the past[24−28] (a brief review is given in ref 16). Here, we recap the main elements of a new scheme that we have formulated recently.[16]

Consider Janak's[29] analytical continuation $\tilde{E}(P)$ of the total electronic energy $E(N)$ of an N(integer)-electron system to a real-valued total electronic charge P. If the occupation numbers of the KS orbitals obey the Fermi−Dirac distribution, $\tilde{E}(P) = E(P)$, where $E(P)$ is the DFT-defined ground-state energy of the system with the total charge P.[29] The binding energy $BE_{HOMO}(P)$ of the most external ("top", "HOMO") *whole* electron charge of this system is defined and can be computed within a chosen version of DFT rigorously

$$BE_{HOMO}(P) = E(P-1) - E(P) \qquad (1)$$

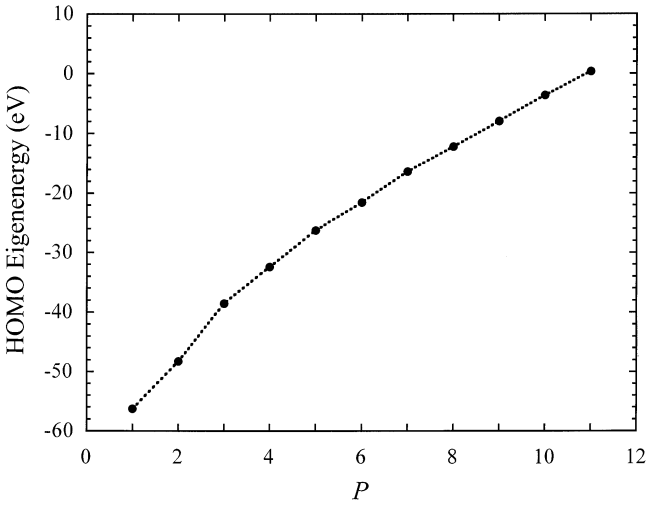

Figure 1. Full circles are the computed KS HOMO eigenenergies of the $Mg_5^{+(10-P)}$ cluster in its +(10-*P*) charge state (*P* is the total valence electronic charge). The dotted lines are the effective HOMO eigenenergies obtained as linear interpolation between neighboring KS HOMO eigenenergies. See the text for details.

One can associate with this top whole electron charge an effective one-particle HOMO eigenenergy $\epsilon^{\text{eff}}_{\text{HOMO}}(P)$ such that

$$\epsilon^{\text{eff}}_{\text{HOMO}}(P = N) = \epsilon_{\text{HOMO}}(N) \tag{2}$$

where $\epsilon_{\text{HOMO}}(N)$ is the true KS HOMO eigenenergy of the *N*-electron system. For any given *N*, one can obtain the values of $\epsilon_{\text{HOMO}}(M)$ for all integers *M*, $1 \le M \le N$, by removing from the system one electron at a time and repeating the DFT computation. In Figure 1 we display, as an example, the values of $\epsilon_{\text{HOMO}}(M)$ for Mg_5^- (full circles). $\epsilon^{\text{eff}}_{\text{HOMO}}(P)$ can then be obtained for any real-valued *P* through interpolation of the $\epsilon_{\text{HOMO}}(M)$ values. The correction $\Delta_{\text{HOMO}}(P)$ needed to convert the effective eigenenergy $\epsilon^{\text{eff}}_{\text{HOMO}}(P)$ into the binding energy of the top whole electron charge is then

$$\Delta_{\text{HOMO}}(P) = BE_{\text{HOMO}}(P) - (-\epsilon^{\text{eff}}_{\text{HOMO}}(P)) \tag{3}$$

When *P* is an integer, eq 3 defines the correction that has to be added to the negative of the KS HOMO eigenenergy of the system to obtain the binding energy of its top electron.

The corrections needed to convert the inner KS eigenenergies into the binding energies of the corresponding electrons are obtained as follows. Define a real-valued grid $\{t\}$ that includes all the integers from 1 to *N*. If the interval δt between the neighboring points of the grid is sufficiently small, then the correction $\Delta_i(N)$, needed to convert the *i*-th KS eigenenergy $\epsilon_i(N)$ of an *N*-electron system into the binding $BE_i(N)$ of the corresponding electron

$$\Delta_i(N) \equiv BE_i(N) - (-\epsilon_i(N)) \tag{4}$$

is well approximated by the linear [in $\alpha_i(N)$] interpolation

$$\Delta_i(N) = \Delta_i(N - \delta t) + [\Delta_{i+1}(N) - \Delta_i(N - \delta t)]\alpha_i(N) \tag{5}$$

where

$$\alpha_i(N) = \frac{\epsilon_i(N) - \epsilon_i(N - \delta t)}{\epsilon_{i+1}(N) - \epsilon_i(N - \delta t)} \tag{6}$$

The meaning of eqs 5 and 6 is quite transparent. If incrementing of the total electronic charge by a small amount δt from $N - \delta t$ to *N* does not shift the KS eigenenergy $\epsilon_i(N - \delta t)$, i.e., $\epsilon_i(N) = \epsilon_i(N - \delta t)$, then $\Delta_i(N) = \Delta_i(N - \delta t)$. If, on the other hand, incrementing of the charge results in $\epsilon_i(N) = \epsilon_{i+1}(N)$, then $\Delta_i(N) = \Delta_{i+1}(N)$. In a typical situation, the value of $\epsilon_i(N)$ is between those of $\epsilon_i(N - \delta t)$ and $\epsilon_{i+1}(N)$. The correction $\Delta_i(N)$ associated with $\epsilon_i(N)$ is then computed as a linear interpolation between $\Delta_i(N - \delta t)$ and $\Delta_{i+1}(N)$.

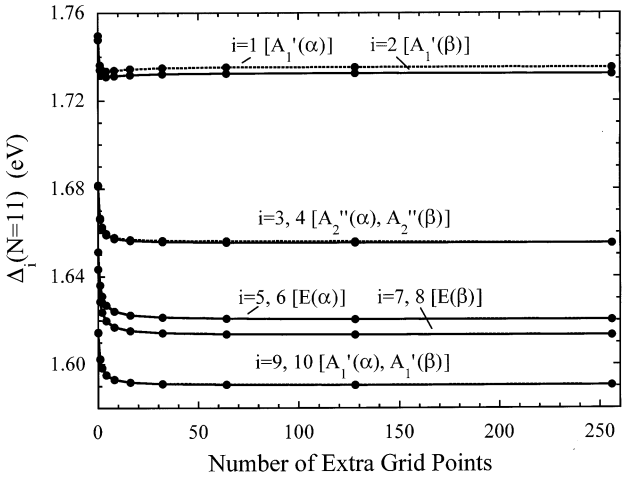

Figure 2. Values of the correction terms $\Delta_i(N)$ for the different (*i*-th) KS eigenenergies of the Mg_5^- cluster (the number of valence electrons $N = 11$) as a function of the number of extra grid points between neighboring integers used in the interpolation procedure, eqs 5 and 6 (see the text for details). The symbols in the brackets are the symmetry labels of the α- and β-spin KS orbitals.

The corrections $\Delta_i(N - \delta t)$ and $\Delta_{i+1}(N)$ in the rhs of eq 5 are themselves defined through recursive application of eqs 5 and 6, until they are reduced to $\Delta_{\text{HOMO}}(t)$ with *t* running over all the grid points between and including $t = i$ and $t = N$. The values of $\Delta_{\text{HOMO}}(t)$ are computed using eq 3. The effective eigenenergies $\epsilon^{\text{eff}}_{\text{HOMO}}(t)$ are to be used in the rhs of eq 6 when the correction $\Delta_{\text{HOMO}}(t)$ appears in the rhs of eq 5. In actual implementations of this scheme one first computes the values of $\Delta_{\text{HOMO}}(t)$, and then propagates these using eqs 5 and 6 as the total charge is gradually increased from *t* to *N*. For further technical details, including those that allow one to reduce the amount of the computational labor associated with the use of the real-valued grid $\{t\}$, we refer the reader to ref 16. Here, we mention only that the scheme proved highly accurate (the computed electron binding energies are on average within 2.5% of the measured values) in applications to atoms and molecules.[16]

In cases, when the gap between the KS eigenenergies is small, sufficiently accurate values of the corrections $\Delta_i(N)$ may be obtained with the grid of integers only. This substantially reduces the scope of the computational task. Figure 2 illustrates the rate of convergence of the corrections associated with the KS eigenenergies of the Mg_5^- cluster. One extra grid point between neighboring integers is sufficient to converge the values of the corrections to 99% or better. If one uses the grid of integers only, then the values are converged to 98% or better. The results on the difference between the binding energies of the two most external electrons in anionic magnesium clusters presented in section 5 are obtained using the grid of integers only.

4. Mg_n and Mg_n^-: Structural Forms

The computed most stable structures of the neutral Mg_n, $n = 2-22$, clusters are shown in Figure 3. The graph of their binding energies per atom is displayed in Figure 4. Mg_2 is only weekly

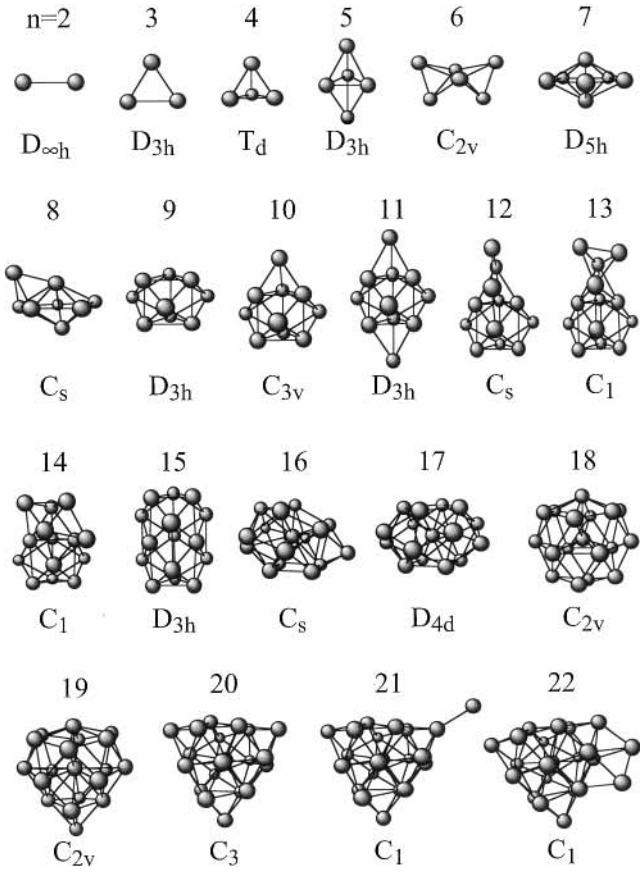

Figure 3. Most stable structures and their symmetries of the neutral Mg_n, $n = 2-22$, clusters.

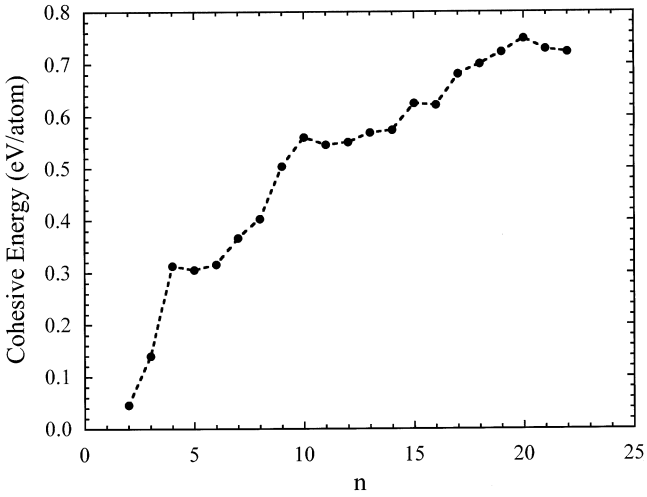

Figure 4. Binding energy per atom of neutral Mg_n clusters.

bound. Starting with Mg_3, however, the binding energy per atom rapidly increases with the cluster size. The most stable configurations of Mg_{4-6} are tetrahedron-based. The structures of Mg_7 and Mg_8 are pentagonal bipyramid-based. The common element in the structures of the Mg_{9-15} clusters is the underlying trigonal prism. The configurations of Mg_{17-22} are derivatives of the structure of Mg_{16}. They are obtained by successive addition of an atom and allowing for relaxations. Overall, these structures agree with or are close to those obtained in earlier studies.[5,7,12,13] The lowest energy configurations of Mg_{15} and Mg_{16}, however, appear to be new. The most stable structures of these clusters, as given by Köhn et al.,[12] emerge as second isomers in our computations. With the exception of Mg_{18}, the most stable configurations of the neutral clusters correspond to the singlet spin-multiplicity state. For Mg_{18} it is a triplet.

Earlier theoretical studies of anionic magnesium clusters[4] covered the range $n = 2-7$ (cf. also ref 13). In agreement with these[4] and the experimental evidence,[30] our computations give an energy of the anion of the Mg atom that is higher than the energy of the neutral atom, which means that Mg^- is not a stable species. The most stable configurations of Mg_n^-, $n = 2-22$, as obtained in our computations, are shown in Figure 5. The structures of Mg_6^- and Mg_7^- are different from those obtained by Reuse et al.[4] These authors define the octahedron as the most stable form of Mg_6^-, and the distorted pentagonal bipyramid as the most stable isomer of Mg_7^-. Both structures emerge in our computations also, but as the second isomer of Mg_6^- and Mg_7^-, respectively. With the exception of Mg_{18}^-, the most stable configurations of the anionic clusters correspond to the doublet spin-multiplicity state. For Mg_{18}^-, it is a quartet.

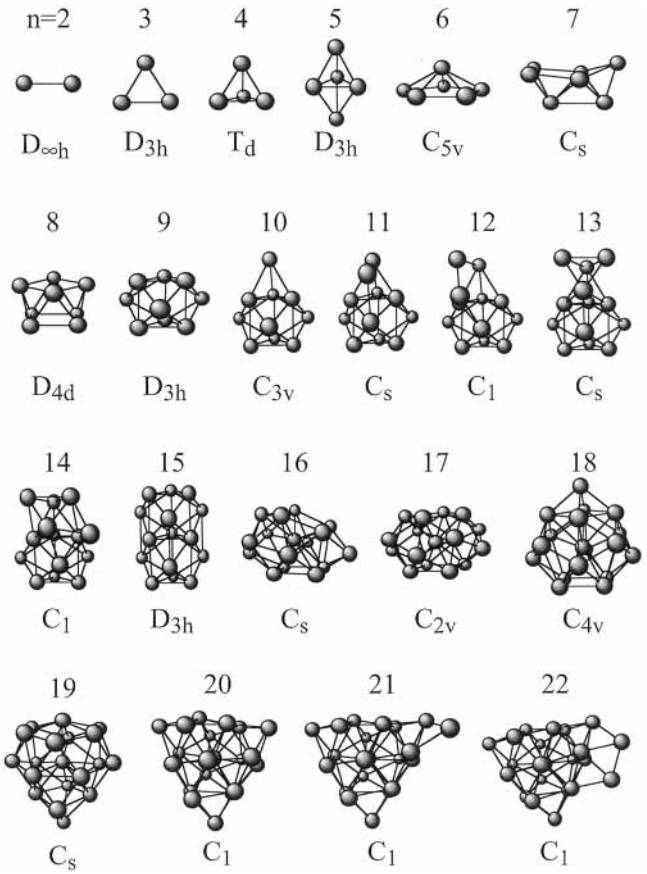

Figure 5. Most stable structures and their symmetries of the anionic Mg_n^-, $n = 2-22$, clusters.

An examination of Figures 3 and 5 shows that although some of the structures of the anionic clusters replicate those of the corresponding neutral cluster, the most stable forms of the anionic species are, in general, different from those of their neutral counterparts. It is this difference that is of particular importance for the analysis of the PES data[15] (cf. next section). More detailed results on the structural characteristics of neutral and charged magnesium clusters, including different isomeric forms, will be given elsewhere.[31]

5. Electronic Features and the Size-Induced Nonmetal-to-Metal Transition

As mentioned, the electronic properties were computed in different charge states, and for each charge state, the native

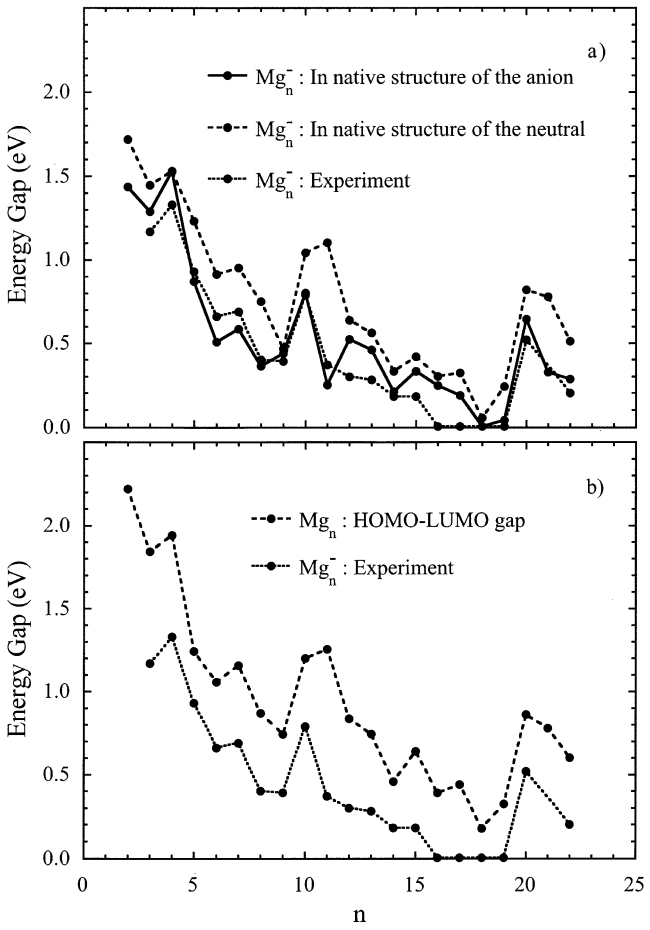

Figure 6. a) The computed and deduced from the experiments[15] difference between the binding energies of the two most external electrons in anionic Mg_n^- clusters; b) The computed HOMO−LUMO gap in neutral Mg_n clusters and the deduced from the experiments[15] difference between the binding energies of the two most external electrons in anionic Mg_n^- clusters.

configuration of the anionic as well as of the neutral cluster was considered. The correction scheme outlined in section 3 was then used to convert the two highest KS eigenenergies of the anionic clusters in the two configurations into the binding energies of the corresponding electrons. (The difference in the zero-point energies of the anionic and neutral clusters, each considered in its native configuration, does not exceed 0.02 eV and was not included in the evaluation of the electron binding energies.) The computed difference in the binding energies of the two most external electrons is plotted in panel a) of Figure 6, which also displays the values of this difference inferred from the measurements.[15] The graphs clearly show that the results obtained considering the Mg_n^- clusters in their native configurations are in very good agreement with the data derived from the experiments. On the other hand, the outcome of computations performed for anions fixed in the native structures of the neutrals is not only quantitatively different, but also it shows qualitatively different local trends. For example, whereas the computed difference in this latter case increases as the cluster size increases from $n = 10$ to $n = 11$, the measured data indicate a decrease. The overall conclusion one arrives at analyzing panel a) of Figure 6 is that the measurements[15] probe the electronic properties of the anionic, rather than the neutral, clusters.

This conclusion, although not unexpected considering that in the experiments the electrons are photodetached from the negatively charged species, is an important one. Its significance becomes clear in light of the following considerations. It is often stipulated that the extra electron occupies the LUMO of the neutral cluster, or more generally, the neutral system at hand. Therefore, it is argued, the difference in the binding energies of the electrons occupying the two highest eigenstates of the anion is the HOMO−LUMO gap of the neutral. This statement, of course, would be true if the structure of the anion were the same as that of the neutral and the eigenenergies of the neutral were not shifting upon addition of an electron. The discussion on the structures above and the results in panel a) of Figure 6 indicate that these conditions do not hold for small magnesium clusters (which, as a rule, is the case for clusters in general), and the photodetachment experiments[15] on Mg_n^- do not measure the HOMO−LUMO gap in the neutral Mg_n clusters. An explicit confirmation of this is given in panel b) of Figure 6, which displays the graphs of the HOMO−LUMO gap in Mg_n considered in their native configurations and of the difference in the binding energies of the two most external electrons in Mg_n^- obtained in the PES measurements. The two are quite different. As is clear from the comparison of the graphs in panels a) and b), the HOMO−LUMO gap of Mg_n is much closer to the computed difference in the binding energies of the two most external electrons in Mg_n^- considered in the native structures of their neutral counterparts. The variance between the two is a consequence of the shifts in the energy levels caused by the addition of an electron.

The HOMO−LUMO gap of finite neutral systems is considered traditionally as the analogue of the gap between the valence and the conduction bands of bulk materials, and the closure of the HOMO−LUMO gap is customarily interpreted as an indication of the transition to a metallic state. In view of this, the above analysis may leave the impression that the photodetachment experiments on finite negatively charged systems contain little, if at all, information on the nonmetal-to-metal transition, since they do not, in general, probe the HOMO−LUMO gap. Such an impression, however, would be misleading. Not only are the PES measurements on anions relevant to this transition, but also they point to an important aspect of it. This aspect is the role of the charge state, which is one of the important consequences and manifestations of the finite-size effects, and which should explicitly be taken into account in the analysis. The geometric and electronic characteristics of the bulk are not affected by addition or withdrawal of electrons, whereas the equilibrium structures and the electron eigenenergies of finite systems may be and, in general, are. The difference between the binding energies of the two most external electrons in anions takes on the role of the HOMO−LUMO gap in the corresponding neutrals, and this difference is as a representative finite-size analogue of the bulk band gap as the HOMO−LUMO gap. Indeed, this difference and the HOMO−LUMO gap approach each other, and both converge to the bulk band gap as the system grows in size.

Another indicator used to analyze the transition to metallicity in magnesium clusters is the extent of the *s*-*p* hybridization, or, alternatively, the degree of the *p*-character of the valence charge distribution. Figure 7 displays the graphs of the latter as evaluated from the Mulliken population analysis. The data are for the anionic and neutral clusters in their respective native configurations, but the results remain largely unchanged when the most stable structures of the neutrals are used for the anions and vice versa. The graphs show that the *p*-character is present in the bonding of even the smallest clusters, but its degree depends on the charge state. This degree changes only weakly with the cluster size in the anionic clusters. The change in the

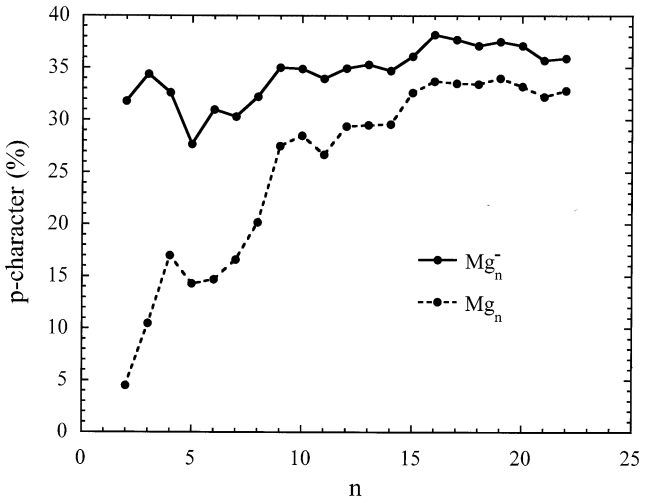

Figure 7. Degree of *p*-character of the valence charge in neutral Mg_n and anionic Mg_n^- clusters, each considered in its native structure.

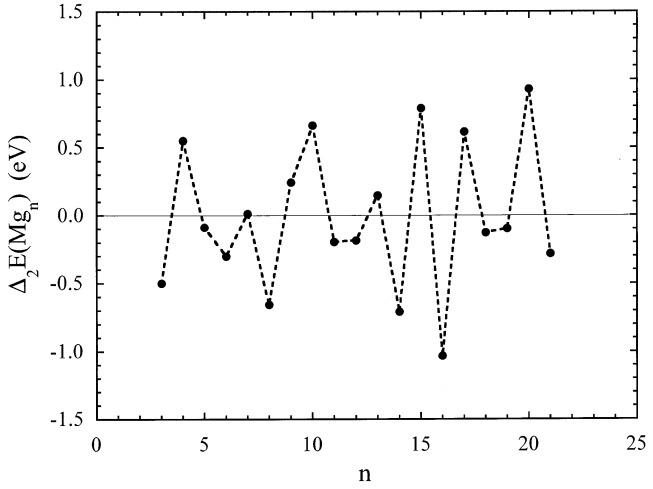

Figure 8. Second difference of the total energies of neutral Mg_n clusters.

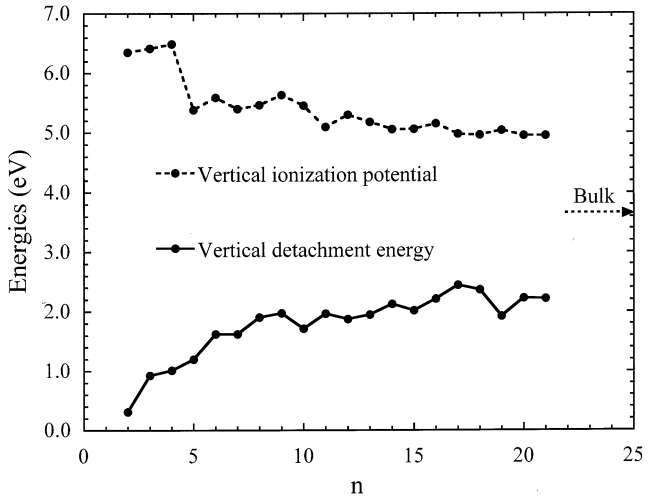

Figure 9. Vertical ionization potential of the neutral Mg_n clusters and the vertical electron detachment energy of the anionic Mg_n^- clusters. The value of the work function of the bulk magnesium is also indicated.

neutral clusters is considerable, and the extent of the *p*-character in Mg_n approaches that in Mg_n^- as n increases. The sensitivity of the degree of the *p*-character to the charge state is another manifestation of the specificity of the finite-size regime. An important implication of this particular manifestation is that the *p*-character of bonding considered in isolation may not be an adequate criterion of the size-induced transition to metallicity. It is the combination of the two changes, the increase of the degree of the *p*-character in Mg_n and the convergence of this degree to that in Mg_n^-, rather than either of the two changes alone, which is significant in the analysis of the transition. For calibration, we note that the degree of *p*-character in the density of states at the Fermi level of bulk magnesium is about 50%.[32]

Next, we touch briefly on the issue of consistency with the jellium model picture. Figure 4 shows local enhancement in the strength of bonding in Mg_n clusters at $n = 4$, 10, and 20, which is consistent with the spherical jellium shell closure at 8, 20, and 40 electrons.[33] A local maximum in the binding energy appears also at $n = 15$, which is consistent with the ellipsoidal shell closure at 30 electrons.[34]

A complementary analysis can be performed in terms of the second difference $\Delta_2 E(Mg_n)$

$$\Delta_2 E(Mg_n) = E(Mg_{n+1}) + E(Mg_{n-1}) - 2E(Mg_n) \quad (7)$$

where $E(Mg_n)$ is the total energy of the Mg_n cluster. Within the jellium model, the maxima of $\Delta_2 E(Mg_n)$ are associated with electronic shell closure.[33] This quantity is also often used as a measure of local stability. The graph of $\Delta_2 E(Mg_n)$ shown in Figure 8 displays maxima at $n = 4$, 10, 15, and 20 (cf. the discussion of Figure 4), as well as at $n = 13$ and 17. The latter two cases correspond to ellipsoidal shell closure at 26 and 34 electrons.[34]

Finally, in Figure 9 we present the vertical electron detachment energies (VDE) computed for the anionic Mg_n^- clusters and the vertical ionization potentials (IP_v) computed for the neutral Mg_n clusters, all considered in their respective native configurations. The anticorrelation between the IP_v and VDE, anticipated from the jellium model for those clusters the neutrals of which have closed electronic shells, holds only for n=20. However, in addition to Mg_{20}, also Mg_4 (but not Mg_{10}, Mg_{13}, Mg_{15}, and Mg_{17}) shows the anticipated increase in the IP_v. And in addition to Mg_{20}^-, also Mg_{10}^-, Mg_{15}^-, and Mg_{17}^- (but not Mg_{13}^-) exhibit the anticipated decrease in the VDE.

The conclusion from the above observations is that magnesium clusters in the size range considered exhibit elements of jellium-like behavior. However, these elements are not fully consistent, at least not within the spherical and ellipsoidal forms of the jellium model. The lack of consistency may be a consequence of the fact that the jellium-like attributes, which have been invoked as yet another indicator of metallicity, are still not fully developed in magnesium clusters smaller than 18−20 atoms (cf. a related discussion on the jellium model and the measured mass-spectra in refs 14 and 15). This would be consistent with the gradual onset of metallic features as discussed above in terms of the difference in the electron binding energies and the degree of *p*-character of the valence charge. But it may also be that the deviations from the jellium behavior reflect, at least in part, only a limited applicability of the jellium model to magnesium clusters. This issue will have to be resolved in future studies.

The overall conclusion from the analysis of the properties of Mg_n and Mg_n^-, $n = 2-22$, clusters presented above is that the changes in their electronic features with the size point to what can be viewed as emergence of metal-like characteristics. It is clear, however, that further studies are needed to unravel the full complexity of the size-induced transition to metallicity. The

emphasis should be on a more detailed understanding of the nature and manifestations of those size-driven changes in the different properties that eventually evolve into the familiar attributes of the bulk insulator-to-metal transition. This understanding should also include the role of the added correlations and dependencies, which are specific to the finite-size regime, and which play no role in the bulk limit. An example is the above-discussed dependence on the charge state, which affects the electronic properties of finite systems directly (shift in the electronic energy levels and change in the character of the charge distribution) and indirectly (change in the native structure) and which has no effect on the bulk insulator-to-metal transition. These added correlations and dependencies cannot be neglected, and it is particularly important to include them in the analysis and interpretation of the results of measurements. To arrive at a comprehensive picture, the studies will have to be extended to clusters of larger sizes. They also will have to address the complex issue of the role of the temperature and the higher energy isomeric forms of the clusters.

6. Summary

In this paper, we presented density functional theory results on the most stable structural forms of Mg_n and Mg_n^-, $n = 2-22$, clusters and a variety of their electronic properties. The difference in the computed binding energies of the two most external electrons in the Mg_n^- clusters considered in their native structures is in very good agreement with the data obtained in the electron photodetachment experiments. The cumulative conclusion from the analysis of this difference, as well as of the changes in the other electronic features of Mg_n and Mg_n^-, is that they are consistent with what can be viewed as emergence of metallic attributes.

The study also leads to some general observations. The finite-size analogue of the bulk insulator-to-metal transition manifests itself in a variety of ways. A comprehensive understanding and description of the phenomenon can be achieved only through the exploration of all its different manifestations, which represent complementary, rather than different but equivalent, aspects and attributes. In this sense, the size-induced transition to metallicity is a richer and more complex phenomenon than the bulk insulator-to-metal transition. The source of the added complexity is the finite-size-specific correlations and dependencies, which become inessential or even irrelevant in the bulk limit. An example of these is the dependence on the charge state. We presented evidence for this dependence in three respects. The first is the shift in the electron energy spectra, the second is the possible change in the energetically preferred structure, and the third is the change in the character of bonding, all caused by changing the charge of the system. Another effect is the existence of different structural forms (isomers) associated with a given cluster size. The role of the isomers will become especially relevant and important in studies directed at understanding the temperature-dependent attributes of the transition.

Acknowledgment. We thank Prof. K. Bowen for stimulating discussions. This work was supported by the Office of Basic Energy Sciences, Division of Chemical Sciences, U.S. Department of Energy under Contract number W-31-109-Eng-38. One of us (P.H.A.) was also supported by CAPES.

References and Notes

(1) See, for example: Moskovits, M. *Annu. Rev. Phys. Chem.* **1991**, *42*, 465. *Clusters of Atoms and Molecules*; Haberland, H., Ed.; Springer-Verlag: Heidelberg, 1994; Vols. 1 and 2. *Theory of Atomic and Molecular Clusters with a Glimpse at Experiments*; Jellinek, J., Ed.; Springer-Verlag: Heidelberg, 1999. *Metal Clusters*; Ekardt, W., Ed.; Wiley: New York, 1999.

(2) Brechignac, C.; Broyer, M.; Cahuzac, P.; Delacretaz, G.; Labastie, P.; Wöste, L. *Chem. Phys. Lett.* **1985**, *120*, 559. Rademann, K.; Kaiser, B.; Even, U.; Hensel, F. *Phys. Rev. Lett.* **1987**, *59*, 2319. Brechignac, C.; Broyer, M.; Cahuzac, P.; Delacretaz, G.; Labastie, P.; Wolf, J. P.; Wöste, L. *Phys. Rev. Lett.* **1988**, *60*, 275. Garcia, M. E.; Pastor, G. M.; Bennemann, K. *Phys. Rev. Lett.* **1991**, *67*, 1142. Haberland, H.; von Issendorf, B.; Yufeng, Y.; Kolar, T. *Phys. Rev. Lett.* **1992**, *69*, 3212. Busani, R.; Folkers, M.; Cheshnovsky, O. *Phys. Rev. Lett.* **1998**, *81*, 3836.

(3) (a) Lee, T. J.; Rendell, A. P.; Taylor, P. R. *J. Chem. Phys.* **1990**, *93*, 6636. (b) Bauschlicher, C. W., Jr.; Partridge, H. *Chem. Phys. Lett.* **1999**, *300*, 364. (c) Klopper, W.; Almlof, L. *J. Chem. Phys.* **1993**, *99*, 5167.

(4) Reuse, F.; Khanna, S. N.; de Coulon, V.; Buttet, J. *Phys. Rev. B* **1989**, *39*, 12911. Reuse, F.; Khanna, S. N.; de Coulon, V.; Buttet, J. *Phys. Rev. B* **1990**, *41*, 11 743.

(5) Kumar, V.; Car, R. *Phys. Rev. B* **1991**, *44*, 8243.

(6) Delaly, P.; Ballone, P.; Buttet, J. *Phys. Rev. B* **1992**, *45*, 3838.

(7) Rothlisberger, U.; Andreoni, W.; Giannozzi, P. *J. Chem. Phys.* **1992**, *96*, 1248.

(8) Gong, X. G.; Zheng, Q. Q.; He, Y. Z. *Phys. Lett. A* **1993**, *181*, 459.

(9) Eriksson, L. A. *J. Chem. Phys.* **1995**, *103*, 1050.

(10) Davidson, E. R.; Frey, R. F. *J. Chem. Phys.* **1997**, *106*, 2331.

(11) Riemann, S. M.; Koskinen, M.; Hakkinen, H.; Lindelof, P. E.; Manninen, M. *Phys. Rev. B* **1997**, *56*, 12 147.

(12) Köhn, A.; Weigend, F.; Ahlrichs, R. *Phys. Chem. Chem. Phys.* **2001**, *3*, 711.

(13) Akola, J.; Rytkonen, K.; Manninen, M. *Eur. Phys. J. D* **2001**, *16*, 21.

(14) Diederich, T.; Döppner, T.; Braune, J.; Tiggesbaunker, J.; Meiwes-Broer, K.-H. *Phys. Rev. Lett.* **2001**, *86*, 4807.

(15) Thomas, O. C.; Zheng, W.; Xu, S.; Shiloh, M.; Bowen, K. H. *Phys. Rev. Lett.*, in press.

(16) Jellinek, J.; Acioli, P. H., submitted for publication.

(17) Becke, A. D. *Phys. Rev. A* **1988**, *38*, 3098.

(18) Perdew, J. P. *Phys. Rev. B* **1986**, *33*, 8822.

(19) Wadt, W. R.; Hay, P. J. *J. Chem. Phys.* **1985**, *82*, 284.

(20) Francl, M. M.; Petro, W. J.; Hehre, W. J.; Binkley, J. S.; Gordon, M. S.; DeFrees, D. J.; Popple, J. A. *J. Chem. Phys.* **1982**, *77*, 3654.

(21) *Handbook of Chemistry and Physics*; Lide D. R., Ed.; CRC Press: Boca Raton, 1993.

(22) Balfour, W. J.; Douglas, A. E. *Can. J. Phys.* **1970**, *48*, 901.

(23) Fuentealba, P.; Szentpaly, L. V.; Preuss, H.; Stoll, H. *J. Phys. B* **1985**, *18*, 1287.

(24) Perdew, J. P.; Zunger, A. *Phys. Rev. B* **1981**, *23*, 5048.

(25) Norman, M. R.; Perdew, J. P. *Phys. Rev. B* **1983**, *28*, 2135.

(26) Trickey, S. B. *Phys. Rev. Lett.* **1986**, *56*, 881.

(27) Akola, J.; Manninen, M.; Hakkinen, H.; Landman, U.; Li, X.; Wang, L.-S. *Phys. Rev. B* **2000**, *62*, 13 216.

(28) Harris, M.; Ballone, P. *Chem. Phys. Lett.* **1999**, *303*, 420.

(29) Janak, J. F. *Phys. Rev. B* **1978,** *18***,** 7165.

(30) Hotop, H.; Lineberger, W. C. *J. Phys. Chem. Ref. Data* **1985**, *14*, 731.

(31) Acioli, P. H.; Jellinek, J., submitted for publication.

(32) Gupta, R. P.; Freeman, A. J. *Phys. Rev. Lett*. **1976**, *36*, 1194. Baraille, I.; Pouchan, C.; Causa, M.; Marinelli, F. *J. Phys.: Condens. Matter* **1998**, *10*, 10 969.

(33) Knight, W. D.; Clemenger, K.; de Heer, W. A.; Saunders: W. A.; Chou, M. Y.; Cohen, M. L. *Phys. Rev. Lett.* **1984**, *52*, 2141.

(34) Clemenger, K. *Phys. Rev. B* **1985**, *32*, 1359.